MULTI-GeV PLASMA ACCELERATION RESULTS AT BELLA*

A. J. Gonsalves †, K. Nakamura, J. Daniels, H.-S. Mao, C. Benedetti, D. E. Mittelberger, E. Esarey, C. B. Schroeder, Cs. Tóth, J. van Tilborg, S. S. Bulanov, C. G. R. Geddes, and W. P. Leemans
Lawrence Berkeley National Laboratory, CA 94708, USA

Abstract

Stable multi-GeV electron beams were obtained in a laser plasma accelerator via precision control over capillary discharge plasma parameters and alignment. The plasma density was determined by measuring the group velocity of laser pulses propagated through the plasma channel. The channel depth was measured using laser centroid oscillations. Improved pointing control was achieved by accurate alignment of capillary angle and position. The pointing fluctuation was 0.6 mrad rms, which was comparable to the electron beam divergence. Simulations showed electron beams in reasonable agreement with experiment via strong self-focusing and injection into multiple plasma periods behind the laser pulse. These processes are strongly parameter dependent, reinforcing the need for precise plasma target control.

INTRODUCTION

Over the past decade laser plasma accelerators (LPAs) [1, 2] have produced electron beams with energy $\gtrsim$ GeV using cm-scale plasmas [3–6], motivating their use for a wide range of light sources [7–12] and as a path towards a TeV-class linear collider [13, 14]. For these and other applications it is important to reduce the laser pulse energy required to reach a given electron energy, since the size and cost of the LPA is dominated by the laser system. A preformed plasma channel can achieve this by mitigating diffraction of the laser beam and extending the acceleration length. In 2006, experiments with laser pulses of energy 2 J demonstrated the generation of electron beams with energy of 1 GeV using a preformed plasma channel [3]. Subsequently other experiments without preformed channels achieved electron beams with tails up to 1.45 GeV with laser energy a few times greater [4]. With the availability of petawatt class lasers, electrons were accelerated in non-preformed plasmas with energy up to 2-3 GeV using laser energy $\approx$ 100 J [5] and 25 J [6].

In this paper two electron acceleration experiments are presented. The first shows the generation of electron beams with energy up to 4.2 GeV using just 16 J of laser energy coupled to a preformed plasma channel [15]. As will be discussed, analysis of the beam parameters on input conditions was complicated by the electron beam angle fluctuation, and the limited angular acceptance of the magnetic spectrometer, which was between ±0.5 mrad and ±1.1 mrad, depending on electron beam energy and applied magnetic field. For the second experiment more accurate capillary alignment techniques were developed and the input laser pulses were spatially filtered to mitigate capillary damage. The electron beam pointing fluctuation was reduced to 0.6 mrad rms, which allowed for consistent observation of electron beams with full-width-half-maximum (FWHM) divergence < 1 mrad.

EXPERIMENTAL SETUP

In the experiments, laser pulses at a wavelength λ = 815 nm with bandwidth 40 nm were generated by the 1 Hz repetition rate Ti:sapphire-based BELLA (BErkeley Lab Laser Accelerator) petawatt laser [16]. The laser pulses were focused to a spot size of $w_0 = 52 \pm 2$ µm (Fig. 1) using an off-axis parabolic mirror with focal length of 13.5 m, where w_0 is defined as the radius at which the intensity decreased by $1/e^2$ of the peak value. The maximum total laser pulse energy delivered at the focal location was $\approx$ 16.6 J, as measured by a power meter inserted into the beam before the off-axis paraboloid. Typical pulse durations at optimum compression were $\tau_0 = 39 \pm 4$ fs (FWHM) as measured by a frequency resolved optical gating (FROG) system. The use of a deformable mirror and wavefront sensor enabled high focal spot quality (Strehl ratio 0.8 ± 0.1) and an associated normalized laser strength $a_0 \gtrsim 1.6$ for 16 J input energy, where $a_0 = 8.5 \times 10^{-10}\, \lambda\,[\mu\text{m}] \sqrt{I_0[\text{W cm}^{-2}]}$ and I_0 is the peak intensity of the laser pulse.

The electron beam profile and position at 11.1 m from the exit of the plasma structure were measured using a calibrated phosphor screen imaged onto a CCD camera. The phosphor screen had field of view ±3 mrad, but only the center ±1 mrad of the electron beam passed through the hole in the optical wedge and power meter. Outside of this angle the electron beam passed through 46 mm of Aluminum and 81 mm of glass, which will approximately double the beam size on the phosphor screen for electron energy of 2 GeV and initial divergence 0.5 mrad. The electron beam energy and charge were measured using a 2.5 m-long magnetic spectrometer of design similar to the spectrometer used in Ref. [3].

As with previous experiments the laser was guided by a capillary discharge plasma channel [17–21] to maximize the electron energy gain [3, 22]. In the present experiments the channel length was increased to 9 cm, and density lowered to between 6×10^{17} cm^{-3} and 11×10^{17} cm^{-3} to increase the acceleration length and electron beam energy. In addition the capillary diameter was increased to 500 µm to minimize damage from the increased laser pulse energy. The capillary discharge was operated with hydrogen using a current pulse of the form $I_{\max} \exp(1 - e^{-t/t_w} - t/t_w)$, where $I_{\max}$ = 250 A and t_w = 88 ns. The laser pulses arrived $\approx$ 30 ns after the peak of the current pulse. Two capillaries

* Work supported by DOE under DE-AC02-05CH11231 and DE-FG02-12ER41798
† ajgonsalves@lbl.gov

ISBN 978-3-95450-168-7

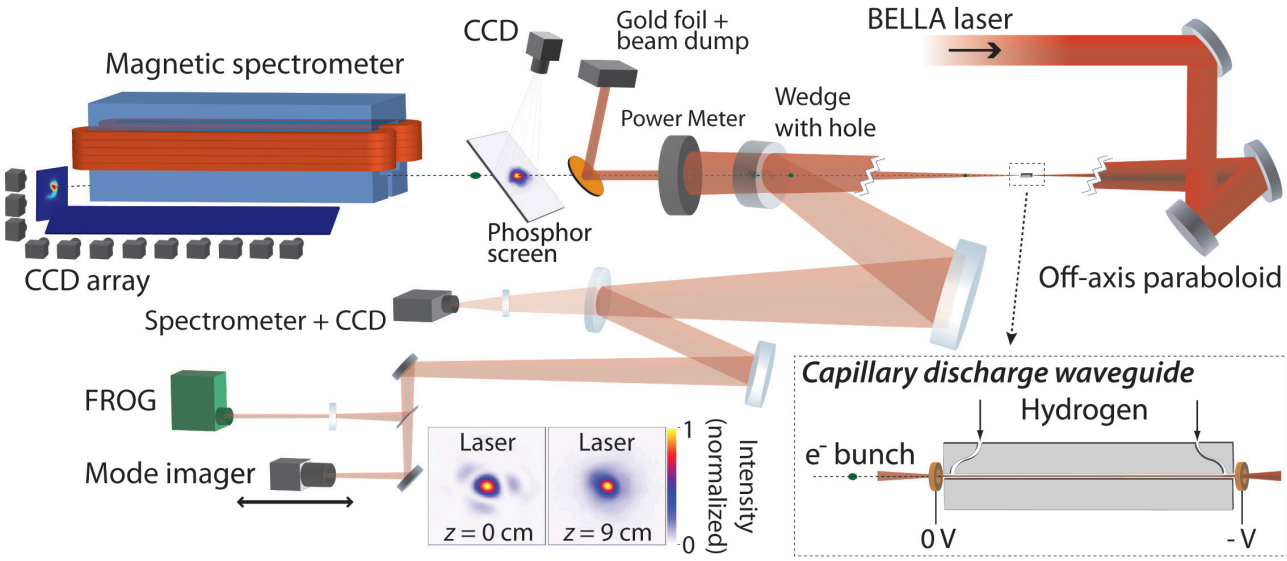

Figure 1: Schematic of the experimental setup showing the target (inset) and diagnostics of the laser and electron beam. Typical laser spatial profiles with input laser pulse energy 16.6 J are shown at focus ($z = 0$) and at the exit of the capillary ($z = 9$ cm) for density 8×10^{17} cm^{-3}. The width of each image is 500 μm.

were employed for the experiments. For capillary A the distance between the capillary ends and the gas feed slots was $L_g = 2$ mm, and for capillary B, $L_g = 6$ mm.

Knowledge of the plasma density and channel profile are essential for understanding laser propagation and electron acceleration. In a capillary discharge waveguide, guiding is achieved in a plasma column with an electron density which increases with radial distance from the axis. To achieve this, a discharge is struck inside a gas-filled capillary. Ohmic heating from the discharge current and cooling at the capillary wall forms an electron density profile that near the axis can be approximated by $n_e(r) = n_e(0) + br^2$ [23]. If the spot size ($1/e^2$ radius of intensity profile) $w_0 = r_m \equiv (\pi r_e b)^{-1/4}$, a laser pulse with a Gaussian transverse profile will propagate through the waveguide with a constant intensity profile [24], where r_e is the classical electron radius.

The on-axis electron density in the plasma channel $n_e(0)$ was determined through measurements of the laser group velocity in a diagnostic setup as described in Refs. [25–27]. Each laser pulse was split into two pulses, one of which was guided by the plasma channel while the other bypassed the target. The pulses were combined after the interaction, and through spectral interferometry the temporal separation of the two pulses was measured. Since the laser group velocity is dependent on the on-axis electron density in the plasma, the delay measurement can be used to retrieve this density [26]. Figure 2 shows the measured relation between density and the neutral H_2 pressure in the capillary before discharge.

The plasma matched spot size was obtained by measuring the laser centroid shift as a function of laser-capillary transverse offset for various initial gas densities and capillary lengths as described in Ref. [28]. An iris of diameter 100 mm was placed at the input of the final pulse compressor,

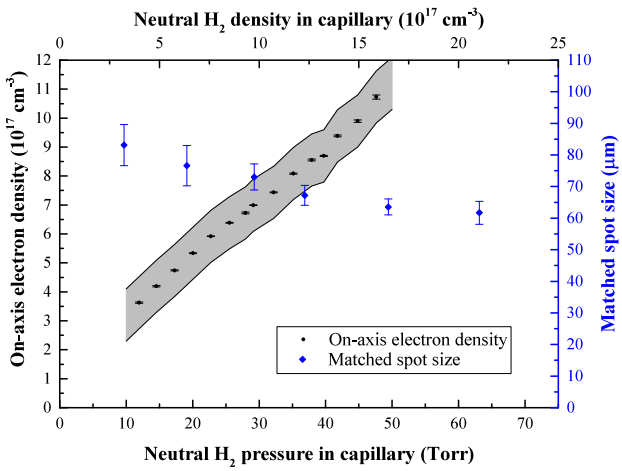

Figure 2: The matched spot size and on-axis density as a function of initial capillary pressure as measured in low-power guiding experiments. The electron density data (black) in the graph are presented as averages for data taken across multiple days, with the standard error indicated by the error bars. The shot-to-shot variation was $\pm 0.2 \times 10^{17}$ cm^{-3} rms. The shaded area indicates the estimated systematic experimental error of 0.9×10^{17} cm^{-3}. The average matched spot size derived from transverse laser centroid oscillations (for various pressures in capillaries of length 3, 6 and 9 cm) is plotted by the blue diamonds. The standard deviation in the measurements at each pressure is shown by the error bars. The shot-to-shot fluctuation for constant parameters was dominated by the laser pointing fluctuation.

resulting in a spot size at focus of 83 μm. This was done to reduce diffraction, ensure the spot size inside the channel remained small compared with the capillary bore for all plasma conditions, and to allow for the non-parabolic profile of the plasma near the capillary wall [20, 23] to be neglected. The laser energy on target was reduced to $\approx$ 150 mJ and pulse length increased to 20 ps to ensure ionization-induced refraction of the laser beam in the gas plume outside the capillary did not occur [29].

The average retrieved matched spot size (for the different capillary lengths, horizontal and vertical directions, and for experiments over several days) is shown in Fig. 2 by the blue diamonds, with the error bars corresponding to the standard deviation of the data. As can be seen from Fig. 2 the matched spot size of the channel varied from $\approx$ 60 to $\approx$ 80 μm, depending on capillary pressure. Since $r_m > w_0$ for all pressures, a contribution from self-focusing at high intensity is needed to optimize guiding.

SIMULATIONS OF ELECTRON BEAM GENERATION

The process of particle self-injection and acceleration was studied by means of PIC simulations performed with the code INF&RNO [30]. The laser and plasma channel parameters were chosen to be close to the experiment parameters. We considered a plasma channel with on-axis density of 6.7×10^{17} cm^{-3} and matched spot size of 82 μm. The laser pulse energy was 16 J and the transverse intensity profile corresponded to a top-hat near-field. The laser was focused at the entrance of the capillary. The summary of the simulation results is presented in Fig. 3. Figure 3(a) shows the evolution of the peak normalized laser field strength as a function of the propagation distance, $a_0(z)$ (solid line), as well as the laser spot size, w_0 (dashed line). At the entrance of the plasma channel the laser-plasma interaction is in the quasi-linear regime, $a_0(0) = 1.66$. Owing to self-focusing and channel guiding, the peak normalized laser field strength reaches $a_0 \simeq 4$ after a propagation distance of $z \simeq 1$ cm. At this point a bubble wake is well formed [see inset (i)], and particle self-injection into several plasma periods behind the laser driver is observed.

Subsequently, the a_0 decreases to a local minimum of $\simeq 2.2$ for $z \simeq 2.3$ cm and, owing to the a_0-dependence of the nonlinear plasma wavelength [1], the size (length) of the wake decreases as shown in inset (ii). For $z \gtrsim 2.5$ cm self-injected bunches continue to be accelerated in the wakefield generated by the laser. The increase of peak normalized laser field strength observed for $z \gtrsim 4$ cm is due to laser self-steepening. Additional self-injection is present for $z \gtrsim 5$ cm and these electrons contribute to the low energy part of the spectrum. For $z \gtrsim 6.5$ cm the pulse length begins to increase and the pulse starts losing resonance with the plasma. At the end of the interaction the 30 % of the laser energy has been depleted. The final electron beam spectrum at the exit of the capillary is shown in Fig. 3(b). The spectrum has been computed considering only the particles with a divergence

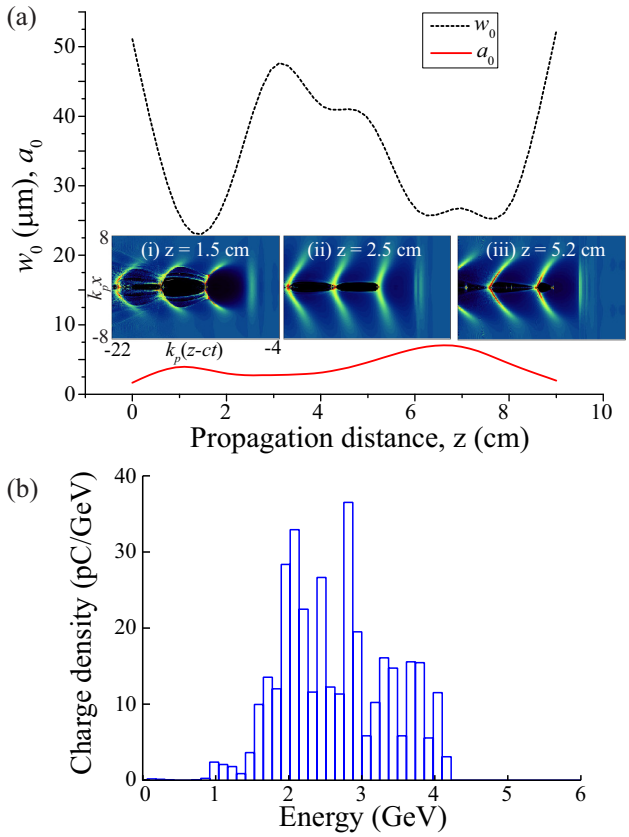

Figure 3: Evolution (a) of the peak normalized laser field strength, $a_0(z)$ (solid line) and spot size w_0 (dashed line), in a PIC simulation for a top-hat laser pulse with an energy of 16 J focused at the entrance of a 9 cm long plasma channel. Snapshots of the wakefield electron density map at various longitudinal locations are shown in (i)-(iii). The spectrum of the electron beam exiting the plasma within a divergence of ±0.5 mrad is shown in (b).

±0.5 mrad, which is approximately the acceptance of the magnetic spectrometer used in the experiments. The total accelerated charge is 43 pC. For these laser-plasma parameters, which yield injection in multiple buckets, the spectrum is broad with maximum electron energy of $\sim$ 4.2 GeV.

The value of the local minimum of a_0 after self-injection depends on the details of the laser-plasma parameters and can strongly affect the final spectrum. For instance, in a simulation with a modestly lower on-axis density of $n_0 = 6.2 \times 10^{17}$ cm^{-3}, the normalized laser field strength reaches the minimum value $a_0 \simeq 2$, and the decrease in plasma wavelength moves the self-injected bunches out of the focusing and accelerating phase of the wake, leading to electron beam loss.

ELECTRON BEAM GENERATION AND POINTING STABILIZATION

In this Section we report on two electron acceleration experiments using pulses from the BELLA petawatt laser coupled into a capillary discharge waveguide. The first ex-

ISBN 978-3-95450-168-7

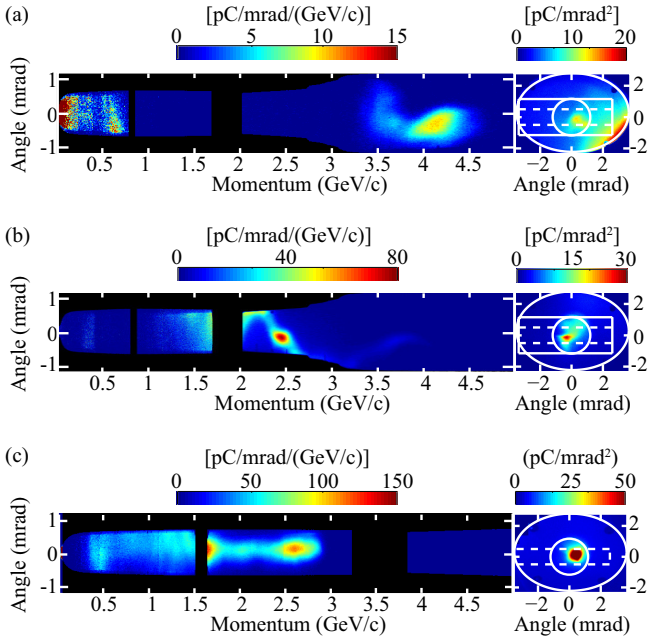

Figure 4: Electron beam energy spectra (left) and spatial profiles (right) for (a) density 7×10^{17} cm^{-3} in capillary A (b) density 6×10^{17} cm^{-3} in capillary A, and (c) density 8.5×10^{17} cm^{-3} in capillary B. The black regions in the magnetic spectrometer images show areas not observable for the applied magnetic field of 0.53 T and1.0 T, for (a/b) and (c), respectively. For the phosphor screen images, the outer white ellipse shows the edge of the phosphor surface and the inner white circle shows the region for which the electron beam passes through the hole in the wedge and power meter. For (a/b) the dashed and solid white rectangles show the acceptance of the magnetic spectrometer for beam energy 2.5 GeV and 3.5 GeV, respectively. For (c) the higher magnetic field results in an acceptance angle that does not vary strongly with energy, and is depicted by the dashed line.

periment employed capillary A, laser energy 16 J, and pulse length 40 fs (peak power of 300 TW). Figure 4(a) shows an example electron beam spectrum and profile for density 7×10^{17} cm^{-3}. The beam energy was $4.2^{+0.6}_{-0.4}$ GeV with 6 % spread (rms), measured charge of 6 ± 1 pC, and divergence of 0.3 mrad (rms). The uncertainty in the electron beam energy was due to the angular acceptance of the spectrometer. The phosphor screen field of view of ±3 mrad allowed for electron beam detection on 99 % of laser shots, but the electron beam pointing fluctuation meant that the majority of charge could be measured on the magnetic spectrometer for just a few percent of shots. An example of one of the best-centered beams is shown in Fig. 4(b), with charge 30 pC. The peak at energy 2.5 ± 0.03 GeV had charge 8.4 ± 1 pC for energy between 2.3 and 2.6 GeV, divergence of 0.5 mrad FWHM, and energy spread 11 %.

Optimization of the accelerator was complicated by laser-induced damage to the capillary. After the experiment measurements of the capillary surface showed that sapphire wall material was eroded near the entrance and re-deposited into the entrance gas feed slot. During high-power operation, this effect was observed by a reduction of flow for a given applied pressure, necessitating the use of the spectral diagnostic of density described in Refs. [15, 31]. Damage to the capillary and plasma profile asymmetry are likely contributors to the $\gtrsim 2$ mrad rms electron beam pointing fluctuations observed.

For the second experiment, several improvements were made to increase the stability of the capillary structure and to reduce electron beam pointing fluctuations. In order to remove some of the energy at larger radii and reduce damage to the capillary, a 0.5 mm-diameter ceramic aperture was placed a few mm from the capillary entrance. This aperture was damaged during high power operation, but it was sufficient to mitigate damage to the capillary for the 960 shots fired. In addition the capillary gas feed slots were moved from 2 mm inside each end (capillary A) to 6 mm (capillary B) to reduce blockage of the entrance slot due to capillary erosion.

The capillary alignment technique was refined to provide more accurate co-linearity of the geometrical axis with the laser axis. In the first experiment, the capillary angle and transverse location were determined by ensuring that displacement by a capillary radius in all directions resulted in equal lowering of the transmitted power of a continuous-wave alignment beam. Asymmetry of the beam and fluctuations in laser power reduce the accuracy of this technique. For the second experiment the capillary angle and transverse location were determined by ensuring that the centroid of the laser pulse exits the capillary with the same position and propagation angle. This technique improved the symmetry of the mode exiting the capillary. Since the alignment and pulsed beams can be offset by ≈ 30 μm, the translation of the capillary is adjusted by up to this amount after switching to the pulsed beam to ensure that the output beam centroid does not vary with capillary pressure. The techniques employed increased the alignment accuracy by a factor of a few to ≈ 20 μm for the capillary transverse position, and few µrad for the capillary angle. It should be noted that translation correction at this stage is more critical than angular correction. For a typical matched spot size of 70 μm, a 30 μm transverse misalignment causes laser angle fluctuations in the waveguide of up to 1.6 mrad. For an angular misalignment of 150 µrad (corresponding to a 2 mm offset at the OAP), the laser angle fluctuations are 150 µrad.

For capillary B (density 8.5×10^{17} cm^{-3} and laser energy 16.6 J) the pointing fluctuation was reduced to 0.6 mrad rms, which allowed for ninety percent of the electron beams to pass through the hole in the wedge and power meter. The beam properties as measured by the magnetic spectrometer were as follows. The charge was 150 pC with standard deviation 17 %, and the peak energy of 2.7 ± 0.1 GeV had standard deviation 3 %. An example electron beam spectrum and profile is shown in Fig. 4(c). The divergence, considering all electron energies, was 0.8 mrad FWHM.

The maximum energy of $\gtrsim 4$ GeV and large energy spread observed are in good agreement with simulations. For simulations at the lowest density, poor guiding results in a decrease in plasma wavelength as the intensity decreases, which causes trapped electrons to enter the defocusing region of the wake. For higher density, as guiding improves, electrons are not lost and the increased wake amplitude leads to higher energy. As the density is increased further, laser depletion and dephasing reduce the maximum energy gain. Self-steepening of the laser enhances dephasing through higher laser intensity and increase in plasma wavelength.

CONCLUSION

The experiments demonstrated that laser pulses with energy of just 16 J propagating in preformed channels can generate multi-GeV electron beams. For density 8.5×10^{17} cm^{-3} the beams had low divergence ($\lesssim 1$ mrad FWHM) and pointing jitter of 0.6 mrad rms. Low pointing jitter is important for realizing LPA applications and for staging LPA modules to achieve higher energy. Possible paths to further reduction of electron beam pointing fluctuations could include reduction in laser pointing jitter and optimizing the capillary length, as well as reduction of pulse front tilt and laser mode asymmetry.

Guiding with lower density is required to increase the dephasing and pump depletion lengths, and hence energy gain. In order to achieve this the required contribution of self-guiding must be reduced. Techniques such as laser heating [32] could achieve this by reducing the plasma channel matched spot size for a given density. Since injection will be suppressed at lower density, techniques to localize injection such as longitudinal density tailoring [33] could then be employed, and simulations indicate that this will allow for the generation of electron beam energies at the 10 GeV level using 40 J, 100 fs laser pulses [34].

ACKNOWLEDGMENT

This work was supported by the Director, Office of Science, Office of High Energy Physics, of the U.S. Department of Energy under Contract No. DE-AC02-05CH11231 and DE-FG02-12ER41798. The authors gratefully acknowledge the technical support from Aalhad Deshmukh, Dave Evans, Mark Kirkpatrick, Art Magana, Greg Mannino, Joe Riley, Ken Sihler, Ohmar Sowle, Tyler Sipla, Don Syversrud and Nathan Ybarrolaza as well as the THALES laser team for the development of the BELLA laser. We also thank Nicholas Matlis, Nadezhda Bobrova, Sergey Bulanov and Krishnan Mahadevan for their contributions and discussions.

REFERENCES

[1] ESAREY, E.; SCHROEDER, C. B.; LEEMANS, W. P. Physics of laser-driven plasma-based electron accelerators. *Rev. Mod. Phys.*, v. 81, p. 1229, 2009.

[2] HOOKER, S. M. Developments in laser-driven plasma accelerators. *Nature Photonics*, v. 7, p. 775, 2013.

[3] LEEMANS, W. P. et al. GeV electron beams from a centimetre-scale accelerator. *Nature Phys.*, v. 2, p. 696–699, October 2006.

[4] CLAYTON, C. E. et al. Self-guided laser wakefield acceleration beyond 1 GeV using ionization-induced injection. *Phys. Rev. Lett.*, v. 105, p. 105003, 2010.

[5] WANG, X. et al. Quasi-monoenergetic laser-plasma acceleration of electrons to 2 GeV. *Nature Communications*, v. 4, p. 1988, 2013.

[6] KIM, H. T. et al. Enhancement of electron energy to the multi-gev regime by a dual-stage laser-wakefield accelerator pumped by petawatt laser pulses. *Phys. Rev. Lett.*, v. 111, p. 165002, 2013.

[7] KNEIP, S. et al. Bright spatially coherent synchrotron x-rays from a table-top source. *Nature Phys.*, v. 6, p. 980, 2010.

[8] CIPICCIA, S. et al. Gamma-rays from harmonically resonant betatron oscillations in a plasma wake. *Nature Phys.*, v. 7, p. 867, 2011.

[9] LEEMANS, W. P. et al. Observation of terahertz emission from a laser-plasma accelerated electron bunch crossing a plasma-vacuum boundary. *Phys. Rev. Lett.*, v. 91, p. 074802, 2003.

[10] MAIER, A. R. et al. Demonstration scheme for a laser-plasma-driven free-electron laser. *Phys. Rev. X*, v. 2, p. 031019, 2012.

[11] TOMASSINI, P. et al. Linear and nonlinear thomson scattering for advanced x-ray sources in plasmonx. *Plasma Science, IEEE Transactions on*, v. 36, n. 4, p. 1782, 2008.

[12] HUANG, Z.; DING, Y.; SCHROEDER, C. B. Compact x-ray free-electron laser from a laser-plasma accelerator using a transverse-gradient undulator. *Phys. Rev. Lett.*, v. 109, p. 204801, 2012.

[13] LEEMANS, W.; ESAREY, E. Laser-driven plasma-wave electron accelerators. *Phys. Today*, v. 62, p. 44, 2009.

[14] SCHROEDER, C. B. et al. Physics considerations for laser-plasma linear colliders. *Phys. Rev. ST Accel. Beams*, v. 13, p. 101301, 2010.

[15] LEEMANS W. P. et al. Multi-gev electron beams from capillary-discharge-guided subpetawatt laser pulses in the self-trapping regime. *Phys. Rev. Lett.*, v. 113, p. 245002, 2014.

[16] LEEMANS, W. P. et al. Bella laser and operations. In: *Proc. of PAC2013*. [S.l.]: JACoW, 2013. p. 1097.

[17] BUTLER, A.; SPENCE, D. J.; HOOKER, S. M. Guiding of high-intensity laser pulses with a hydrogen-filled capillary discharge waveguide. *Phys. Rev. Lett.*, v. 89, p. 185003, 2002.

[18] SPENCE, D. J.; HOOKER, S. M. Investigation of a hydrogen plasma waveguide. *Phys. Rev. E*, v. 63, p. 015401, 2000.

[19] SPENCE, D.; BUTLER, A.; HOOKER, S. First demonstration of guiding of high-intensity laser pulses in a hydrogen-filled capillary discharge waveguide. *Journal of Physics B: Atomic, Molecular and Optical Physics*, v. 34, p. 4103, 2001.

[20] GONSALVES, A. J. et al. Transverse interferometry of a hydrogen-filled capillary discharge waveguide. *Phys. Rev. Lett.*, v. 98, p. 025002, 2007.

[21] JAROSZYNSKI, D. et al. Radiation sources based on laser–plasma interactions. *Philosophical Transactions of the Royal Society A: Mathematical, Physical and Engineering Sciences*, v. 364, p. 689, 2006.

[22] IBBOTSON, T. P. A. et al. Laser-wakefield acceleration of electron beams in a low density plasma channel. *Phys. Rev. ST Accel. Beams*, v. 13, p. 031301, 2010.

[23] BOBROVA, N. A. et al. Simulations of a hydrogen-filled capillary discharge waveguide. *Phys. Rev. E*, v. 65, p. 016407, 2002.

[24] SPRANGLE, P. et al. Propagation and guiding of intense laser pulses in plasmas. *Physical Review Letters*, APS, v. 69, n. 15, p. 2200, 1992.

[25] TILBORG, J. van et al. Measurement of the laser-pulse group velocity in plasma waveguides. *Phys. Rev. E*, v. 89, p. 063103, 2014.

[26] SCHROEDER, C. B. et al. Group velocity and pulse lengthening of mismatched laser pulses in plasma channels. *Phys. Plasmas*, v. 18, p. 083103, 2011.

[27] DANIELS, J. et al. Plasma channel diagnostics for capillary discharges. In: *Advanced Accelerator Concepts Workshop Proceedings 2014*. [S.l.: s.n.].

[28] GONSALVES, A. J. et al. Plasma channel diagnostic based on laser centroid oscillations. *Phys. Plasmas*, v. 17, p. 056706, 2010.

[29] LEEMANS, W. P. et al. Experiments and simulations of tunnel-ionized plasmas. *Phys. Rev. A*, v. 46, p. 1091, 1992.

[30] BENEDETTI, C. et al. Numerical investigation of electron self-injection in the nonlinear bubble regime. *Phys. Plasmas*, v. 20, p. 103108, 2013.

[31] SHIRAISHI, S. et al. Physics of laser-driven plasma-based electron accelerators. *Phys. Plasmas.*, v. 20, p. 063103, 2013.

[32] BOBROVA, N. A. et al. Laser-heater assisted plasma channel formation in capillary discharge waveguides. *Phys. Plasmas*, v. 20, p. 020703, 2013.

[33] GONSALVES, A. J. et al. Tunable laser plasma accelerator based on longitudinal density tailoring. *Nature Phys.*, v. 7, p. 862, 2011.

[34] LEEMANS, W. P. et al. The BErkeley Lab Laser Accelerator (BELLA): A 10 GeV Laser Plasma Accelerator. In: *Advanced Accelerator Concepts*. [S.l.]: AIP, 2010. v. 1299, p. 3.